Solid State Sciences 148 (2024) 107435

Contents lists available at ScienceDirect

Solid State Sciences

journal homepage: www.elsevier.com/locate/ssscie

Exploring the physical properties of cubic $CsGeBr_{3-n}I_n$ (n= 0, 1, 2, 3) compounds: Ab initio calculations of perovskites prospective for the application in solar cells

Anas Y. Al-Reyahi [a], Ahmad Mufleh [b,*], Said M. Al Azar [c], Mufeed Maghrabi [a], Nabil Al Aqtash [a], Saber Saad Essaoud [d,e], Khadidja Berarma [f], Adel Shaheen [a], Mohammed Elamin Ketfi [g], Ahmad A. Mousa [h]

[a] Department of Physics, Faculty of Science, The Hashemite University, P. O. Box 330127, Zarqa, 13133, Jordan
[b] Preparatory Deanship, Prince Sattam Bin Abdulaziz University, Al-Kharj, Saudi Arabia
[c] Department of Physics, Faculty of Science, Zarqa University, Zarqa, 13132, Jordan
[d] Department of Physics, Faculty of Science, University of M'sila, 28000, M'sila, Algeria
[e] Laboratoire de Physique des Particules et Physique Statistique, Ecole Normale Supérieure-Kouba, BP 92, Vieux-Kouba, 16050, Algiers, Algeria
[f] Department of Chemistry, Faculty of Science, University of M'sila, 28000, M'sila, Algeria
[g] Department of Electronics, Faculty of Technology, University of M'sila, 28000, M'sila, Algeria
[h] Department of Basic Sciences, Middle East University, Amman, 11831, Jordan

ARTICLE INFO

Keywords:
Cubic perovskite solar cells
Optoelectronic properties
Solar cell
Hybrid functional

ABSTRACT

The cubic perovskites $CsGeBr_{3-n}I_n$ (n = 0, 1, 2, 3) were investigated using the density functional theory (DFT) for their structural, electronic, and optical properties. The present DFT calculations are carried out using three models for exchange-correlation potential, namely PBE, mBJ, and YS-PBE0. The bandgap decreases in the above sequence of compounds except $CsGeBrI_2$, which reveals the smallest bandgap. The mBJ approximation has a larger bandgap than the PBE and smaller than the YS-PBE0. Results of calculations within the YS-PBE0 approach for $CsGeBr_3$ and $CsGeI_3$ agree well with QSGW + SO results. The $CsGeBr_{3-n}I_n$ compounds are direct bandgap semiconductors and CBM and VBM are positioned at the R point and determined mainly by Ge s-states and Br(I) p-states, respectively. Analysis of optical properties shows that the DFT calculations within the PBE model consistently produce the highest static dielectric function values, while the YS-PBE0 method gives the smallest values. The curves of optical coefficients shift toward lower energies when decreasing the Br atoms in $CsGeBr_{3-n}I_n$. The studied compounds are semitransparent in the infrared and visible regions and show promising potential for photovoltaic applications, including solar cells.

1. Introduction

Numerous research studies have indicated that perovskites are promising candidates for usage in photovoltaics and other renewable energy technologies [1–10]. The name perovskite was originally given for calcium titanium oxide (CaTiO3). Thereafter any material with a similar crystal structure and has the chemical formula ABX_3 is called perovskite, where A and B are cations whereas X stands for an anion that ties them together [11–13]. Perovskite structures can be constructed using a variety of materials by choosing different combinations of A, B, and X, which allows researchers to fine-tune the physical, optical, and electronic properties of materials [13–18].

Organic-inorganic hybrids perovskite solar cells have made exceptional advancements in power-conversion efficiency (PCE) in the last decade due to their superior optoelectrical properties [19]. However, a major obstacle to their commercialization is the instability induced by the volatile organic components. To create a chemically stable inorganic perovskite, the $CsPbI_3$ compound has demonstrated its ability to produce efficient solar cell devices, where Cs is used to offset the chemical volatility associated with the usage of the organic cations in methylammonium as well as formamidinium lead iodide perovskites [20]. In this regard, increasing attention has been paid to the inorganic

* Corresponding author.
E-mail address: ahmad_mufleh@yahoo.com (A. Mufleh).

https://doi.org/10.1016/j.solidstatesciences.2023.107435
Received 30 September 2023; Received in revised form 16 December 2023; Accepted 30 December 2023
Available online 30 December 2023

compounds cesium lead triiodide ($CsPbI_3$), and cesium lead tribromide ($CsPbBr_3$) due to their superior thermal stability, apposite direct bandgap (about 1.7 and 2.3 eV), and exceptional optoelectronic characteristics like the power conversion efficiency (PCE) of about 20.32 %, [21–23]. It is worth mentioning that cesium lead trichloride ($CsPbCl_3$) also reveals very prospective optoelectronic properties [24].

The physical properties of $CsGeBr_3$ and $CsGeI_3$ compounds were extensively studied experimentally as well as theoretically. In addition, the compounds' stability was examined over time under different ambient conditions. $CsGeBr_3$ was synthesized by Tang et al. [25] and tested using x-ray diffraction and reflection powder second-harmonic generation method. Their results show that $CsGeBr_3$ has a rhombohedral structure with excellent nonlinear optical efficiency. In addition, they apply *ab initio* calculations to examine the second-order nonlinear susceptibilities of $CsGeBr_3$. They concluded that the rhombohedral $CsGeBr_3$ is a potential material to be utilized in infrared nonlinear optics. Mahmood et al. [26] investigated the mechanical, optical, thermoelectric, and thermodynamic properties of cesium-based bromides for applications in energy-renewable devices using the most thorough DFT-based *Wien2k* code. Their density functional theory (DFT) calculations demonstrate that the optical properties exhibit a high degree of sensitivity to variations in the visible band gap and the materials exhibit high thermoelectric efficiency. The electronic structure of the perovskite crystal $CsGeI_3$ was analyzed by Tang et al. [27] through the utilization of first-principles calculations. The obtained results are subsequently compared with the available experimental data. Their calculations demonstrate that $CsGeI_3$ possesses a direct-transition energy gap measuring 0.74 eV. Almishal et al. [7] have studied the lead-free trigonal $CsGeI_{3-x}Br_x$ mixed-halide perovskite system for optoelectronics using first-principles calculations with the PBE energy exchange potential. The optical properties of $CsGeI_{3-x}Br_x$ exhibited anisotropic behavior, with a notable negative correlation between the Ge-X bond length and the bandgap.

In this study, the Br atom in cubic perovskite of $CsGeBr_{3-n}I_n$ (n = 0, 1, 2, 3) was replaced by I atom in different ratios to examine the effect of such replacement on their structural, elastic, electronic, and optical properties using different exchange-correlation potentials and draw a comparison between the results of the various exchange-correlation potentials. *Wien2k ab-initio* code was utilized to examine the physical properties of $CsGeBr_{3-n}I_n$ (n = 0, 1, 2, 3). Evaluation of the structural and electronic properties of the compounds was facilitated by calculating the lattice parameters (*a*), atomic positions, density of states (DOS), and band structures. The elastic properties were examined by evaluating the elastic constants (C_{11}, C_{12}, and C_{44}), bulk, shear and Young's moduli, Poisson's ratio, Debye temperature, and elastic sound velocity. Finally, the optical properties were quantified by calculating the dielectric constant, refractive index, reflection, and absorption coefficient.

This study aims to analyze the physical properties of $CsGeBr_{3-n}I_n$ to assess their suitability for use in solar cells and optoelectronic devices. The investigation will be conducted computationally using mainly Wien2K. Unlike previous studies on some of these compounds as mentioned, this study will utilize different exchange-correlation potentials such as PBE, mBJ, and YS-PBE0 some of which have not been previously explored. The results obtained from these potentials, particularly mBJ and YS-PBE0, are expected to closely align with the experimental results. Additionally, our research focuses on analyzing previously unexplored compounds that possess unique characteristics and produce exceptional results.

2. Computational details

The *wien2k* simulation package was used to solve the Kohn-Sham (KS) equation using Full Potential Linearized Augmented Plane Wave (FP-LAPW) [28]. The structural, electronic, and optical properties of $CsGeBr_{3-n}I_n$ (n = 0, 1, 2, 3) were studied using different exchange-correlation potentials like the Perdew-Burke-Ernzerhof (PBE), Tran-Blaha modified Becke-Johnson (TB-mBJ), and hybrid functionals (YS-PBE0). All calculations were carried out using the FP-LAPW approach. An extensive description of the equations that govern the various exchange-correlation potential types can be found in the literature [28–38].

Within the field of electronic structure calculations, various exchange-correlation potentials are crucial for solving the Kohn-Sham equation. The Perdew-Burke-Ernzerhof (PBE) functional, which is extensively employed for its computational efficiency and dependable performance, effectively accounts for the exchange and correlation interactions in a well-balanced manner. The modified Becke-Johnson (mBJ) potential is highly effective in enhancing the precision of band gaps, particularly for semiconductors and insulators. The Yukawa Screened-PBE0 (YS-PBE0) hybrid functional integrates a screening parameter into the PBE0 framework, resulting in improved characterization of the electronic properties [28,36,38,39].

The maximum value of the reciprocal lattice vectors (K_{max}) is set to (8.0), and the smallest radius of the Muffin-Tin (MT) spheres (R_{MT}) is equal to 2.5 a. u. The selected k-point mesh is 15 × 15 × 15 which includes the Brillouin region. Atomic electronic configurations have been divided into two distinct types: core electrons and valence electrons. The valence electron for Cs is the $6s^1$ electron, for Ge it is the $4s^2p^2$ electron, and for both Br and I it is the 3 d^{1o} $4s^2$ $4p^5$ electron. To separate the core and valence states, a cut-off energy of −6 Ry was used to generate the free atomic density. The atomic force cutoff in structural optimization is 1.0 mRy/Bohr. Core/valence energy = (−6.0 Ry) and nn = 2 indicate a difference in energy of −6.0 Ry, where nn denotes nearest neighbor distance. Furthermore, the highest charge density in the Fourier series is $G_{max} = 14$ (a.u.)$^{-1}$. The iterative procedure is repeated until the calculated total energy and charge are less than (0.0001 Ry) and (0.0001 e), respectively. Spin-orbit calculations were neglected due to the weak spin-orbit coupling of the Ge atom compared to the Pb or Sn atoms. Scalar relativistic approximation was used for valence electrons, whereas fully relativistic effects were taken into account for in the case of core electrons.

The Birch-Murnaghan equation of state was used to calculate the optimized structural parameters for the compounds, which include the lattice constant (*a*), bulk modulus (B_0), ground state energy (E_0), and unite cell volume (V_0) [1,29,30,40]. The electronic properties, such as the band structure and Density of States (DOS), were calculated using the optimized structural parameters [28]. Bandgap was determined using the above-mentioned exchange-correlation potentials. The optical properties of the compounds were also investigated using PBE, mBJ, and hybrid functionals exchange-correlation potential (YS-PBE0) to gain valuable information about their structure. We have also examined the optical properties of $CsGeI_{3-n}Br_n$, by calculating the absorption coefficient α(ω), reflectivity R(ω), refractive index n(ω), and the real and imaginary parts of the complex dielectric function. The equations that govern the optical properties are fully described and explained elsewhere [1,29–31,41].

3. Results and discussion

3.1. Structural properties and dynamic stability

The present section focuses on investigating the structural properties and dynamic stability of the cubic perovskite $CsGeBr_{3-n}I_n$ (n = 0, 1, 2, 3) within the Pm3 m (#221) space group. The unit cells for these structures are illustrated in Fig. 1, where the alternatives a, b, c, and d correspond to the different values of n (i.e., the number of iodine atoms). The geometric calculations were conducted during the stage of volume optimization, which involve the determination of the minimum volume that corresponds to the minimum energy. The Birch-Murnaghan equation of state is used to calculate the optimized structural parameters. The calculated parameters are listed in Table 1 together with previous theoretical [42] and experimental [6] values. Table 1 shows that our

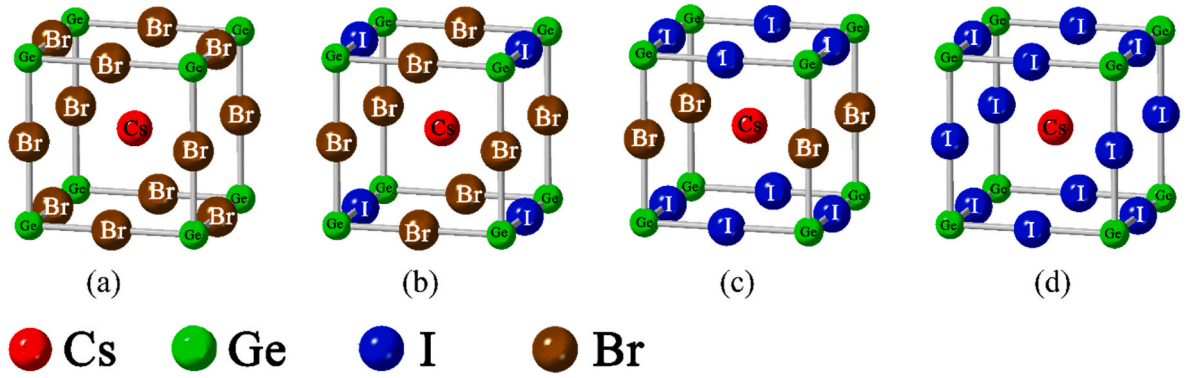

Fig. 1. The unit cell of $CsGeBr_{3-n}I_n$ (n = 0, 1, 2, 3), where a, b, c, d refer to n = 0, 1, 2, 3 respectively.

Table 1
Lattice constant a (Å), optimum volume V_0 (Å^3), bulk modulus B (GPa), and minimum energy E_0 (Ry) for Pm-3m (#221) $CsGeBr_{3-n}I_n$ (n = 0, 1, 2, 3).

Compound	Space group		a (Å)	V0 (Å^3)	B (GPa)	E0 (Ry)	E_{form} (eV/atom)	E_{coh} (eV/atom)
CsGeBr3	Pm-3m (#221)	This Work	5.603	1187.25	21.94	−35419.02	−0.984	2.472
		Theoretical	5.407 [47]					
		Experimental	5.69 [6]					
$CsGeBr_2I$		This Work	5.753	1284.84	20.61	−44443.80	−0.702	2.211
$CsGeBrI_2$		This Work	5.874	1367.48	20.14	−53468.59	−0.617	1.973
$CsGeI_3$		This Work	5.991	1451.36	16.60	−62493.39	−0.586	1.757
		Theoretical	5.783 [47]					
		Experimental	6.05 [6]					

computed values for the equilibrium lattice parameter for $CsGeBr_3$ and $CsGeI_3$ reasonably fit with the values obtained from previous theoretical [42] and experimental [6] works. To the best of our knowledge there are no experimental or theoretical values for $CsGeBr_2I$ and $CsGeBrI_2$ to compare with. The lattice parameter '*a*' shows a systematic increase from 5.603 (for n = 0) to 5.991 (for n = 3). The replacement of bromine by iodine leads to an increase in the lattice parameters and volume, which can be attributed to the larger ionic size of iodine [43]. In addition, such replacement results in a decrease in both the bulk modulus and the minimum energy. The inverse correlation between the bulk modulus and the unit cell volume confirms the observed results [1].

To analyze the dynamic stability, the phonon frequency modes at the Γ point [44] have been calculated using a finite differences methodology using VASP code [1,44]. It has been observed that the vibrational frequencies of the lowest energy structures of $CsGeBr_{3-n}I_n$ (n = 0, 1, 2, 3), as depicted in Fig. 2, exhibit solely positive values without any presence of imaginary components. Hence, it can be inferred that all structures are stable.

The evaluation of the compounds' stability was conducted by calculating the cohesive energy (E_{coh}) and the formation energy (E_{form}). A positive E_{coh} value indicates thermodynamic stability, while a negative E_{form} value signifies chemical stability. The cohesive energy was calculated using the formula: $E_{coh} = (E_{Cs} + E_{Pb} + (3\text{-}n)E_{Br} + nE_I - E_{tot})$/ total number of atoms, where E_{tot} represents the total bulk energy of $CsPbBr_{3-n}I_n$ (n = 0,1,2,3) compounds, while E_{Cs}, E_{Pb}, E_{Br}, and E_I denote the total energies of isolated Cs, Pb, Br, and I atoms, respectively. On the other hand, the formation energy (E_{form}) for $CsPbBr_{3-n}I_n$ compounds was calculated using the formula: $(E_{tot} - (E_{Cs} + E_{Pb} + (3\text{-}n)E_{Br} + nE_I))$/total number of atoms. The calculated values for both E_{coh} and E_{form} are summarized in Table 1. Thermodynamic stability was demonstrated by the obtained positive cohesive energies for $CsPbBr_{3-n}I_n$ (n = 0,1,2,3): 2.472, 2.211, 1.973, and 1.757 eV/atom. Likewise, the chemical stability of these compounds was confirmed by the negative formation energy values of −0.984, −0.702, −0.617, and −0.586 eV/atom for $CsPbBr_{3-n}I_n$ (n = 0,1,2,3) [33,45,46].

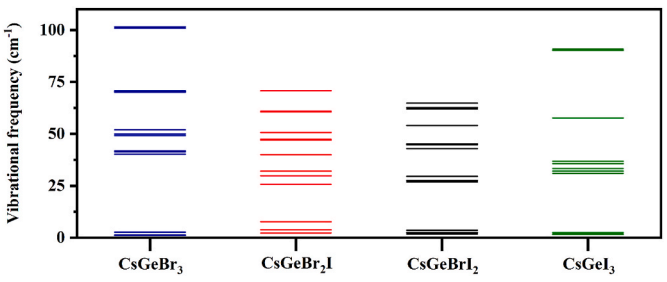

Fig. 2. The vibrational frequencies (3N–6) of the lowest energy for CsGeBr3-nIn (n = 0, 1, 2, 3) structures.

3.2. Electronic properties

Table 2 presents our theoretically calculated bandgap values for $CsGeBr_{3-n}I_n$ (n = 0, 1, 2, 3) using PBE, mBJ, and YS-PBE0 exchange-correlation potentials together with some available theoretical and experimental optical bandgap values that were previously published by other research groups. From Table 2, we note that our YS-PBE0 results

Table 2
The bandgap in eV for $CsGeBr_{3-n}I_n$ (n = 0, 1, 2, 3) using PBE, mBJ, and YS-PBE0 exchange-correlation potentials together with the previously published data.

Compound	Bandgap (eV)				
	Prev./Theo [48].	Expt [50].	PBE	mBJ	YS-PBE0
$CsGeBr_3$	0.867[a], 1.948[b], 1.800[c], 0.710[d]	2.32	0.742	1.040	1.497
$CsGeBr_2I$			0.565	0.851	1.266
$CsGeBrI_2$			0.476	0.744	1.148
$CsGeI_3$	0.746[a], 1.404[b], 1.199[c], 0.465[d]	1.53	0.595	0.756	1.267

[a] LDA.
[b] QSGW.
[c] QSGW + SO.
[d] QSGW + SO at LDA lattice parameter.

(for both $CsGeBr_3$ and $CsGeI_3$) are very close to the QSGW + SO results [47]. It should be mentioned here that QSGW is one of the most accurate methods for bandgap estimation. It is worth mentioning here that the best agreement between the experimental findings and the DFT calculations in perovskite containing Si, Ge, Sn, and Pb [47] is observed when the DFT calculations are carried out including the spin-orbit coupling. However, according to Huang and Lambrecht [47], the spin-orbit splitting decreases for lighter elements (i.e., lower atomic number). They found that the bandgap for $CsGeBr_3$ and $CsGeI_3$ decreased from 1.948 eV to 1.404 eV–1.800 eV and 1.199 eV, respectively when SO coupling was included in the calculations. Furthermore, the use of the mBJ and YS-PBE0 functionals probably is quite sufficient for the comparative study of changes in the electronic structure when substituting bromine atoms by iodine atoms in cubic $CsGeBr_{3-n}I_n$ (n = 0, 1, 2, 3) compounds. However, recent achievements in DFT computations indicate that the best agreement of the experiments and theory in semiconducting compounds consisting of Cs/Ge/Br/I atoms, like in the present case, is observed when the DFT calculations are carried out using, in particular, TB-mBJ functional and including also the spin-orbit coupling effect and the Hubbard correction parameter U for strongly correlated electrons. Certainly, such DFT calculations are timely rather expensive [48,49]. Note that $CsGeBr_3$ exhibits a wider bandgap as compared with other compounds irrespective of the exchange-correlation potential used to estimate the bandgap. This result agrees with the result obtained by Huang and Lambrecht [2], where the bandgap increases with increasing the halogen electronegativity. The bandgap of $CsGeBr_2I$ is comparatively smaller than that of $CsGeBr_3$, while still being larger than the bandgap of the remaining two compounds. The compound $CsGeBrI_2$ was ultimately found to possess the smallest bandgap.

Our choice of modified Becke-Johnson (mBJ) to represent the results in this study is based on its intermediate nature between PBE and YS-PBE0, as illustrated in Fig. 3. Nevertheless, the variations among these energy exchange potentials are minimal, with the primary distinctions lying in the bandgap and sometimes in the peak height. Fig. 4 illustrates the band structure and the total density of states (T-DOS) for $CsGeBr_{3-n}I_n$ (n = 0, 1, 2, 3) compounds, employing the mBJ potential. The band structures of the four compounds are quite similar. Huang and Lambrecht [2] reported that the band structure of $CsGeX_3$ has unique features called orbital inverted, where the valence band maximum (VBM) occurs at R (k-point) and consists of anti-bonding states between Ge s-states and halogen (Br or I) p-states. The non-degenerate dispersing VBM leads to Ge s-state characters. At the conduction band minimum (CBM), the threefold degeneracy of Ge p-states occurs. The corresponding values of the bandgaps are presented in Table 2. The analysis of the band structure indicates that the compounds exhibit direct bandgap along the R path, which indicates a high degree of consistency between our results and those reported in previous studies [27].

Fig. 5 illustrates the partial density of states (PDOS) for $CsGeBr_{3-n}I_n$ using the mBJ exchange-correlation potential. The primary contribution in the negative energy region is attributed to Br and I ions, whereas Ge ions contribute more to the positive energy region. On the other hand, the contribution of Cs to the total density of states (TDOS) is minimal.

The primary contribution pertaining to the distribution of states in the DOS for each atom in $CsGeBr_{3-n}I_n$ is illustrated in Fig. 6. In all investigated compounds the contribution of Cs's came from its d state, whereas Ge's contribution was observed from its p state. The p state was observed to be the source of contribution for both Br and I ions in all compounds. Moreover, in $CsGeBr_3$ and $CsGeBr_2I$, Br contributes through the $p_x + p_y$ orbitals, while in $CsGeBrI_2$, it contributes through the p_z orbital. Iodide, on the other hand, contributes through the p_y orbital in $CsGeBr_2I$, and through the $p_x + p_y$ orbitals in $CsGeBrI_2$ and $CsGeI_3$.

3.3. Optical properties

The optical characteristics of $CsGeBr_{3-n}I_n$ (n = 0, 1, 2, 3) were examined through a comprehensive analysis of several important parameters including dielectric functions $\varepsilon_1(\omega)$ and $\varepsilon_2(\omega)$, absorption $\alpha(\omega)$, energy loss function $L(\omega)$, refractive index $n(\omega)$, extinction coefficient $k(\omega)$, reflectance $R(\omega)$, and optical conductivity $Re(\sigma)$ and $Im(\sigma)$. Calculations were carried out using the PBE, mBJ, and YS-PBE0 approaches. The investigated compounds were exposed to incoming photons with energy ranging from 0 to 13.5 eV. The predicted equilibrium lattice constant was utilized to determine the optical properties of the compounds. Fig. 7 provides a comparative analysis of the calculated optical parameters for $CsGeBr_3$ using the various exchange-correlation potentials. The main point to note from Fig. 7 is that the YS-PBE0 parameterization of exchange-correlation potential has a different behavior than the other parameterizations, especially at high energy. From the figure of ε_1, the static values were decreased from 7.0 to 5.0 to 3.3 when the exchange-correlation potential parameterization varies from PBE to mBJ to YS-PBE0, respectively.

3.3.1. Optical complex dielectric function

The optical complex dielectric function $[\varepsilon(\omega) = \varepsilon_1(\omega) + i\,\varepsilon_2(\omega)]$ is a fundamental parameter that characterizes the interaction of the material with the incident electromagnetic radiation [51]. The real $\varepsilon_1(\omega)$ and imaginary $\varepsilon_2(\omega)$ components of the dielectric function offer valuable information regarding the material's capacity to absorb and transmit light. The real part $\varepsilon_1(\omega)$ reflects the portion of the dielectric constant that is associated with energy storage. The measurement of $\varepsilon_1(\omega)$ quantifies the extent to which an externally applied electric field can induce polarization in the material [52]. A larger value of $\varepsilon_1(\omega)$ is indicative of increased polarization and enhanced energy storage capacity. The regulation of a material's capacitance has a significant impact on its electrical characteristics, such as the accumulation of

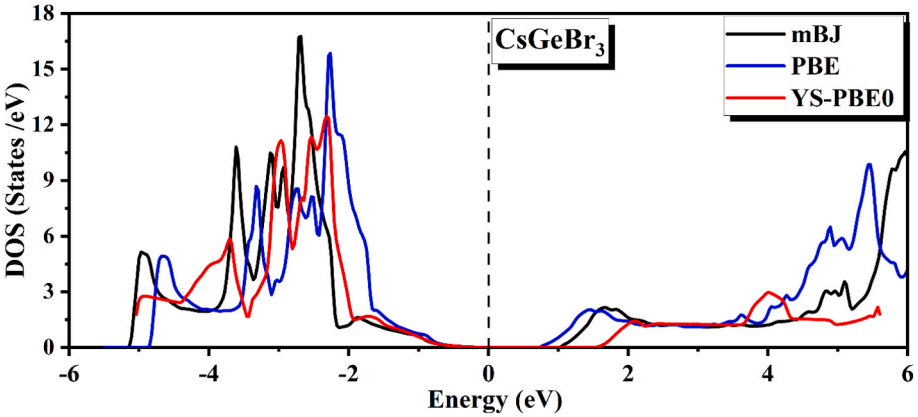

Fig. 3. The total density of states (TDOS) of $CsGeBr_3$ using PBE, mBJ, and YS-PBE0 exchange-correlation potentials.

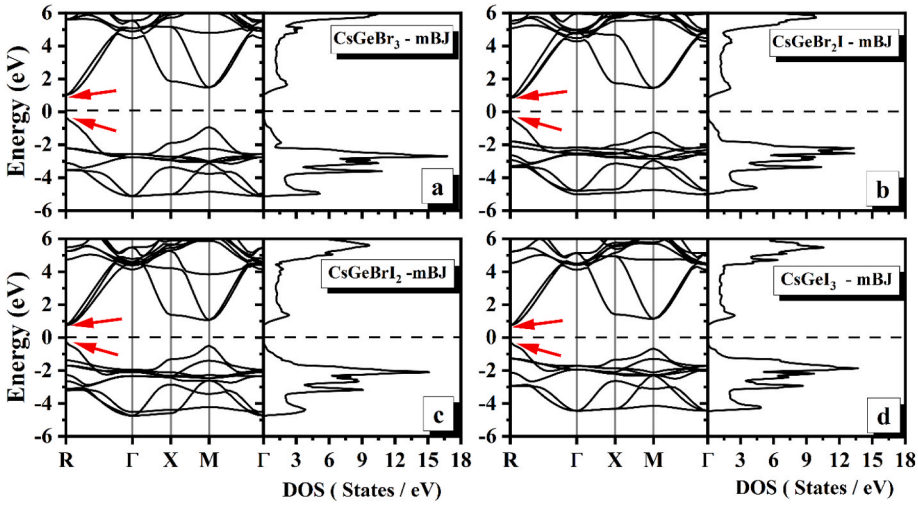

Fig. 4. mBJ calculations of the total density of states (TDOS) and band structure (BS) for $CsGeBr_{3-n}I_n$ (n = 0, 1, 2, 3).

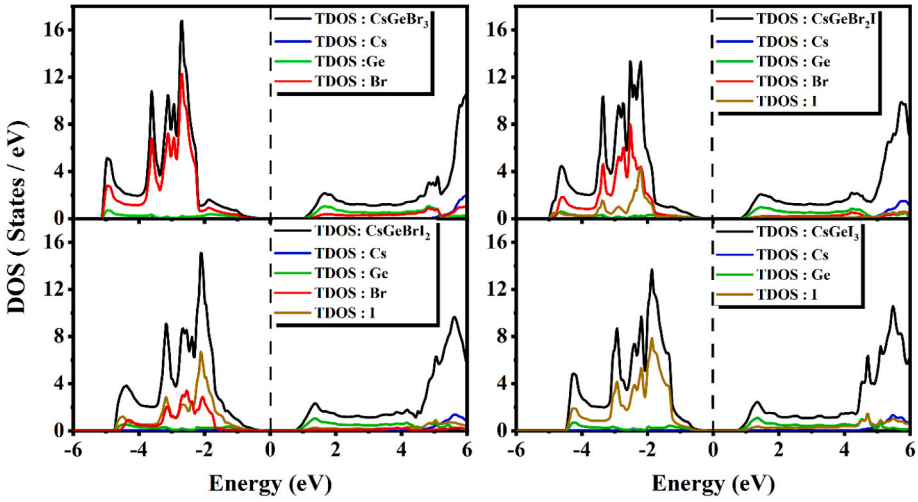

Fig. 5. mBJ calculations of the total density of states (TDOS) for $CsGeBr_{3-n}I_n$ (n = 0, 1, 2, 3) and the constituting atoms.

charge and the transmission of electromagnetic waves. The energy loss or energy dissipation is connected to the imaginary component $\varepsilon_2(\omega)$. The energy dissipation results from several factors, such as conduction, dielectric relaxation, and resistive losses. When the magnitude of the complex permittivity, $\varepsilon_2(\omega)$, is not equal to zero, the material exhibits absorption characteristics by converting a portion of the energy carried by the electric field into thermal energy.

The real and imaginary parts of the dielectric function are the key parameters from which other optical properties can be derived [28]. Fig. 8 displays the variations of $\varepsilon_1(\omega)$ and $\varepsilon_2(\omega)$ as a function of the incident photon energy using the various exchange-correlation potentials.

The values of the optical parameters at a given energy/energy range that can be deduced from Fig. 7 are summarized in Tables 3 and 4 (see the supplementary information). The static dielectric function, denoted as ε_1 (0), represents the real dielectric function at 0 eV. It is worth mentioning here that the PBE usually produces the highest values for the static dielectric function. This behavior can be ascribed to the inherent constraints within the PBE framework to accurately describe the electronic correlation effects, which results in an underestimation of the dielectric response. On the other hand, YS-PBE0 distinguishes itself by yielding the lowest values for the static dielectric function. YS-PBE0 method takes into account the integration of a portion of the Hartree-Fock exchange, which improves the handling of electron-electron interaction and leads to a more precise characterization of the dielectric response [28,36]. This observation aligns with the Penn model [53], which posits that a smaller energy bandgap is associated with ε_1 (0), while a larger energy bandgap corresponds to a lower value of ε_1 (0). Additionally, it can be observed that PBE exhibits the most prominent peak values (see Table 4 in the supplementary information). Electronic transitions and the material's intrinsic energy band structure play a key role in explaining why $\varepsilon_1(\omega)$ appears in the negative region. The perturbation of the dielectric response of the material occurs when electrons undergo transitions from occupied to unoccupied states within a defined energy range, leading to a reduction in the value of $\varepsilon_1(\omega)$. The observed decrease in ε_1 can be ascribed to the influence of electrons transitioning from the valence band to the conduction band, which impacts the polarizability of the material in a way that opposes the typical dielectric characteristics [30,54]. A comprehensive examination and comprehension of this distinctive behavior are vital in developing materials that possess customized optical characteristics that may be applied in many scientific and technological fields. In contrast to the other chemicals investigated, $CsGeBrI_2$ has the largest value of ε_1 (0) and the highest peak maximum.

In the subsequent figures, the mBJ method is selected to represent the calculated optical parameters because of its intermediate outcomes

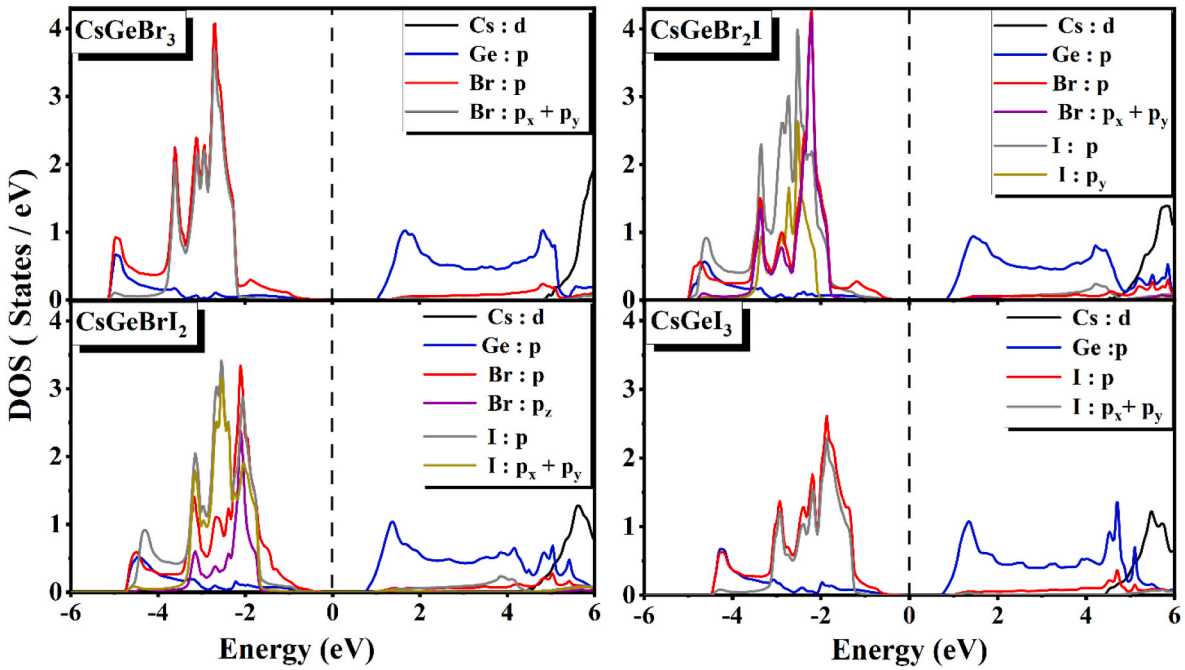

Fig. 6. mBJ calculations of the main contribution states for each atom in the density of states (DOS) for each compound in $CsGeBr_{3-n}I_n$ (n = 0, 1, 2, 3).

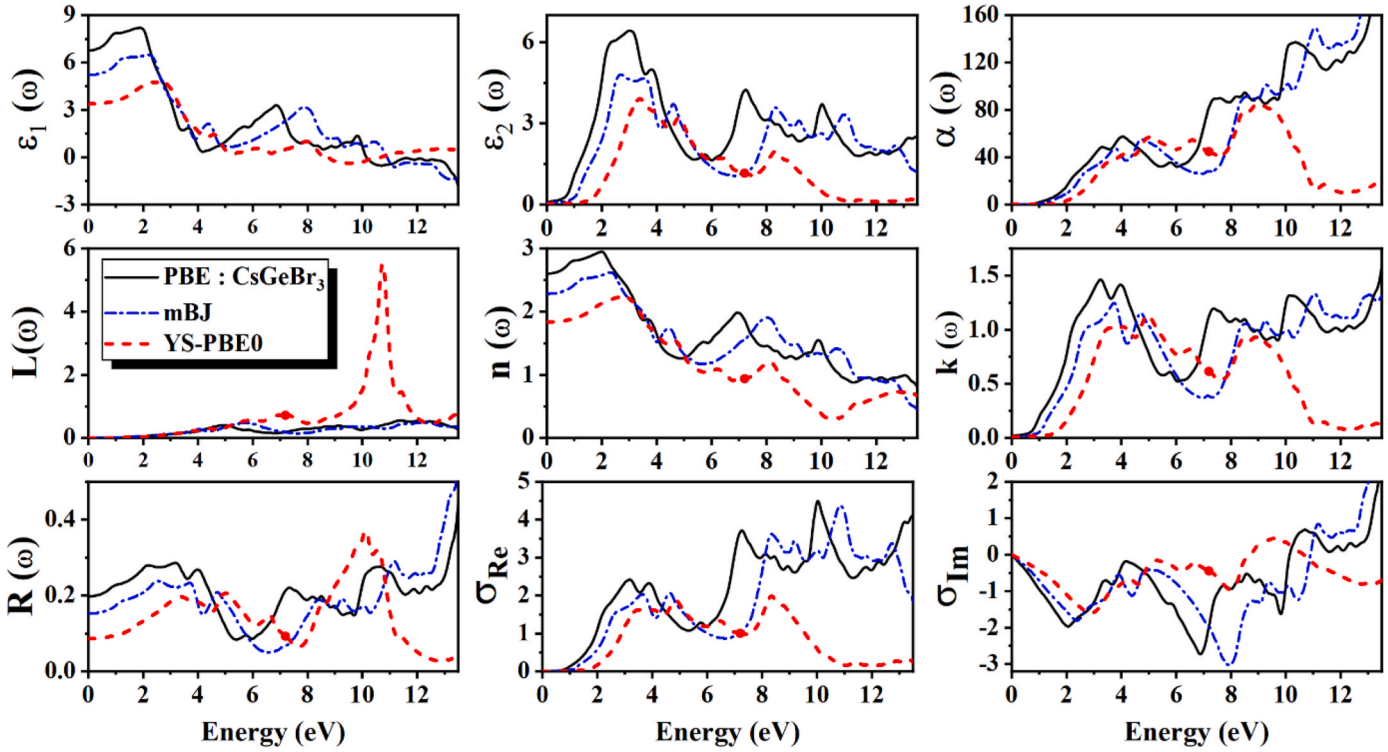

Fig. 7. Real and imaginary dielectric functions $\varepsilon_1(\omega)$ and $\varepsilon_2(\omega)$, absorption $\alpha(\omega)$, energy loss function $L(\omega)$, refractive index $n(\omega)$, extinction coefficient $k(\omega)$, reflectance $R(\omega)$, and complex optical conductivity $\sigma_{Re}(\omega)$ and $\sigma_{Im}(\omega)$ using PBE, mBJ, and YS-PBE0 for $CsGeBr_3$.

between the PBE and YS-PBE0 methods. Fig. 9 shows the variations of $\varepsilon_1(\omega)$ and $\varepsilon_2(\omega)$ as a function of the incident energy for the studied compounds using the mBJ potential. Our results exhibit a significant level of consistency with the findings of previous studies [26].

3.3.2. *Optical conductivity*

Optical conductivity measures the electrical conductivity of the material when it interacts with light. The real component of optical conductivity possesses significant physical implications, operating as a crucial metric for assessing the material's capacity to conduct electrical current in reaction to incident light. This statement explains the degree to which electrons can engage in collective oscillations when subjected to the effects of an external electromagnetic field. The peaks depicted in Fig. 10a and the maximum peak values (see Table 4 in the

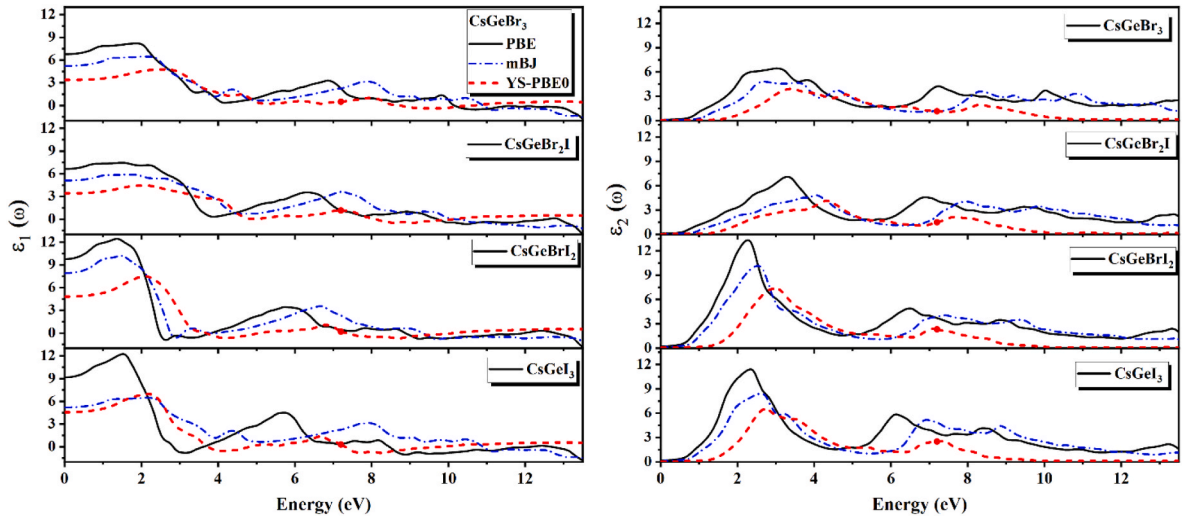

Fig. 8. **(a)** Real and **(b)** imaginary dielectric functions of the studied compounds as a function of incident energy using PBE, mBJ, and YS-PBE0.

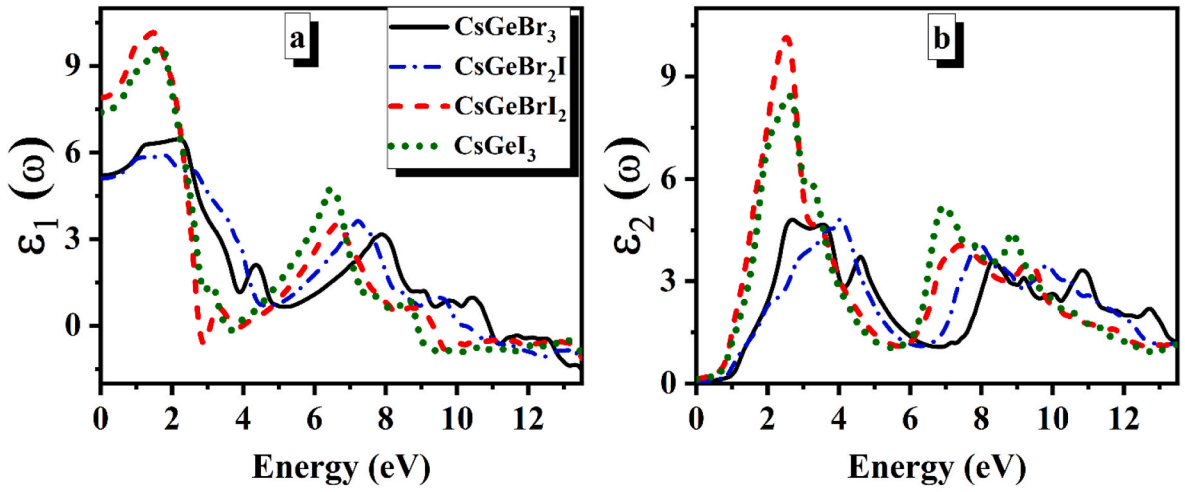

Fig. 9. **(a)** Real and **(b)** imaginary dielectric functions as a function of the incident energy using the mBJ potential.

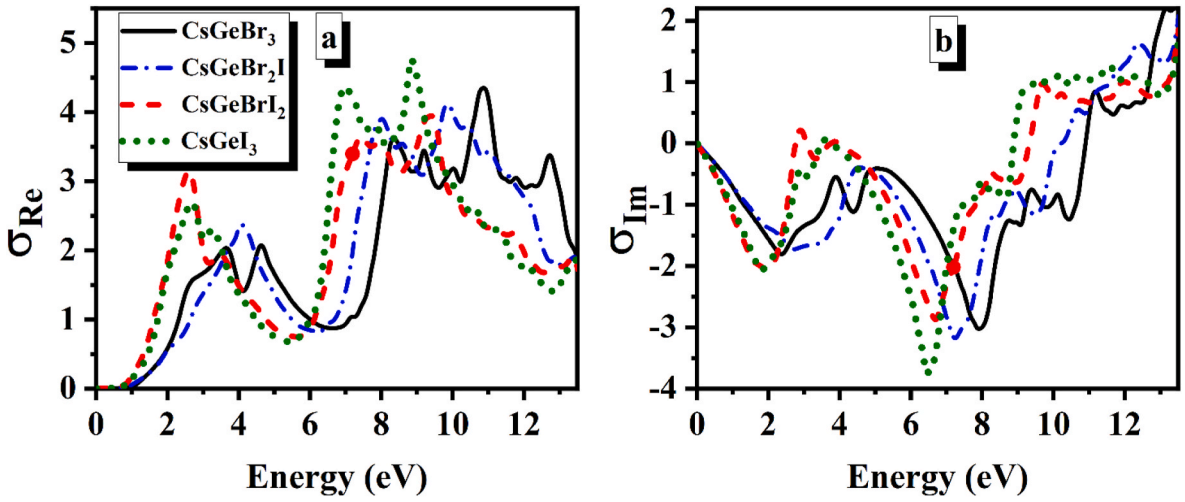

Fig. 10. **(a)** Real and **(b)** imaginary electric conductivities as a function of incident energy using the mBJ potential.

supplementary information) provide vital insights into the electrical structure of the material and its transition properties. This phenomenon denotes a resonance effect in which the electrons of the material assimilate energy from the incident light, causing them to move to higher energy levels. In contrast, the imaginary component of optical conductivity provides insight into the absorption capability of the material. A negative value, as illustrated in Fig. 10b, indicates that the material demonstrates a surplus of energy acquired from the incident photons, leading to energy depletion inside the system. The observed phenomenon of negative absorption indicates the presence of stimulated emission, hence suggesting the material's potential for applications such as lasing or photon amplification [55]. The observed pattern exhibits similarities to the Drude-Lorentz model, a theoretical framework that characterizes the reaction of unbound electrons to external stimuli. The comprehension of the real and imaginary parts of the optical conductivity and their correlation with the Drude-Lorentz model provides insight into the complex interaction between electrons and photons, facilitating the interpretation of the fundamental principles that determine the optical characteristics of the material [56].

3.3.3. The refractive index and extinction coefficient

The refractive index and extinction coefficient provide insights into the material's ability to bend and absorb light, respectively [57]. Fig. 11 illustrates the relationship between the real component of the complex refractive index n(ω) and the imaginary component k(ω) as a function of energy. The refractive index is known as the real component, whereas the extinction coefficient is commonly referred to as the imaginary part. The optical property k(ω) holds significant importance in several photoelectric applications like solar cells, photodetectors, and spectroscopy [58–60]. Fig. 11 illustrates an inverse relation between n(ω) and the incident energy whereas the extinction coefficient k(ω) shows a direct relation. Both n(ω) and k(ω) show the same general trend for all studied compounds, with $CsGeBrI_2$ displaying the highest values of n(ω) and k (ω), especially at the peak maximum, (seeTable 4 in the supplementary information). Fig. 11 shows that the $CsGeBrI_2$ compound exhibits the largest static refractive index n (0) value between the studied compounds. In general, the material with a high refractive index shows more polarization because the incident photons interact with more electrons. Note that n (0) and ε_1 (0) are coupled through the formula $n^2(0) = \varepsilon_1(0)$ [61].

The absorption coefficient α(ω) and reflectivity R(ω) provide insight into the proportion of incoming energy that is absorbed and reflected, respectively, thereby revealing the overall transparency or opacity of the material [52,57]. The absorption coefficient α(ω) is a crucial parameter that provides significant insights into the interaction between

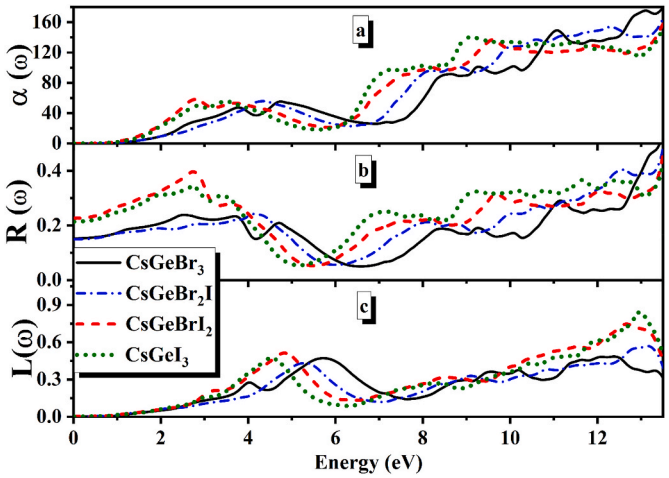

Fig. 12. (a) absorption coefficient **(b)** reflectivity, and **(c)** the energy loss function versus incident photon energy using mBJ.

electromagnetic radiation and material substances [52,57,62]. The measurement estimates the amount to which a substance absorbs electromagnetic radiation when exposed at a particular frequency ω. Fig. 12a depicts α(ω) versus energy. In general, as the incident energy increases, the value of α(ω) increases, which means the ability of the material to absorb the incoming light is enhanced. The reflectivity R(ω) exhibits a similar tendency to α(ω) as shown in Fig. 12b. Additionally, $CsGeBr_3$ demonstrates the highest value when employing PBE and mBJ, while it achieves the maximum value with YS-PBE0. In addition, the energy-loss spectrum L(ω) can capture the specific energy range within which the material exhibits optimal absorption of incident radiation, typically corresponding to notable electronic transitions [63]. The general trend of Fig. 12c is the increase of absorption by increasing the incident photon energy, with the exception of the energy range 5–7eV where the absorption has a minimum value. The general trend that applies to all optical parameters (see Figs. 9–12) is that the curves shift to lower energy as the number of Br atoms decreases from three to zero.

The examination of the absorption coefficient α(ω), reflectivity R(ω), and energy loss function L(ω) is very crucial in order to provide valuable insights into the optical characteristics of the compounds. The reflectivity, R(ω), exhibits minimum reflection within the energy range of 5–7 eV and maintains low values in the energy range of 0–3 eV. The appearance of R(ω) within these specific energy intervals indicates a significant degree of light reflection and limited energy absorption. On

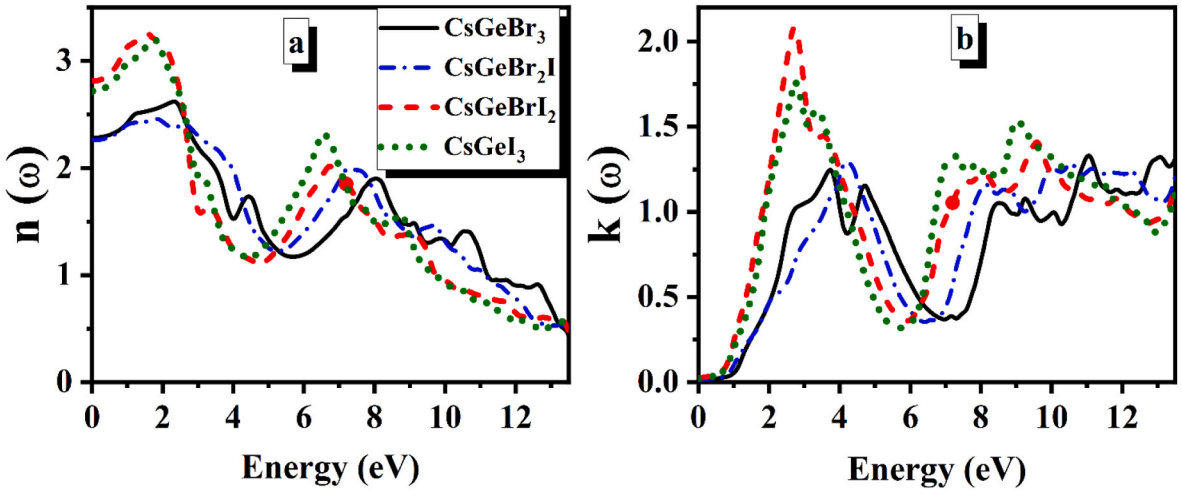

Fig. 11. (a) Refractive index and **(b)** Extinction coefficient as a function of the incident energy using the mBJ potential.

the other hand, the absorption behavior was found to be restricted within the energy range 0–3 eV, suggesting a partially transparent state in the infrared and visible regions of the electromagnetic spectrum. Additionally, the energy loss function L(ω) indicates a minimum within the energy range 0–3 eV, providing additional evidence for the semi-transparent characteristics of the materials in this spectral region. Based on the results shown in Fig. 12 it can be inferred that the studied compounds exhibit some degree of semitransparency in the infrared and visible regions of the electromagnetic spectrum, thereby indicating their potential suitability for various optical applications.

4. Conclusions

The present study investigates the structural, electronic, and optical characteristics of the cubic perovskites $CsGeBr_{3-n}I_n$ (n = 0, 1, 2, 3) through the utilization of the density functional theory (DFT). Various exchange-correlation potentials, including PBE, mBJ, and YS-PBE0, were employed during the calculations. The lattice parameter exhibits an increase when the Br atoms are replaced by I atoms, while the bulk moduli experience a decrease. The density of states (DOS) analysis reveals that the bandgap experiences a decrease when the Br atoms are substituted by I atoms with the exception of $CsGeBrI_2$, which shows the lowest bandgap value. The PBE approximation exhibits the lowest bandgap followed by the mBJ, whereas the YS-PBE0 produces the highest bandgap value. The YS-PBE0 results for both $CsGeBr_3$ and $CsGeI_3$ show excellent agreement with the QSGW + SO results. The examination of the band structure reveals that the compounds demonstrate a direct bandgap along the R path from the interaction between Ge s-states and halogen (Br or I) p-states. The analysis of the optical properties reveals that the PBE consistently yields the highest values for the static dielectric function, whereas the YS-PBE0 method yields the lowest ones. The obtained data are consistent with the Penn model. The compound $CsGeBrI_2$ demonstrates a higher value of n (0) in comparison with other compounds. The studied compounds exhibit an increase in the absorption coefficient as a result of the replacement of Br atoms with I atoms except for $CsGeBrI_2$. Also, the studied compounds demonstrate a certain level of semitransparency across the infrared and visible regions. The obtained results suggest that the cubic perovskites $CsGeBr_{3-n}I_n$ (n = 0, 1, 2, 3) exhibit promising potential as viable options for the forthcoming photovoltaic applications, including solar cells.

CRediT authorship contribution statement

Anas Y. Al-Reyahi: Conceptualization, Data curation, Formal analysis, Supervision, Writing – original draft, Writing – review & editing, Methodology, Visualization. **Ahmad Mufleh:** Conceptualization, Supervision, Visualization, Writing – review & editing. **Said M. Al Azar:** Conceptualization, Funding acquisition, Investigation, Methodology. **Mufeed Maghrabi:** Validation, Writing – review & editing. **Nabil Al Aqtash:** Validation, Visualization. **Saber Saad Essaoud:** Validation, Visualization. **Khadidja Berarma:** Data curation, Resources. **Adel Shaheen:** Data curation, Formal analysis, Validation. **Mohammed Elamin Ketfi:** Validation, Writing – review & editing. **Ahmad A. Mousa:** Resources, Software.

Declaration of competing interest

The authors of this article declare no conflict of interest.

Data availability

Data will be made available on request.

Acknowledgment

This study is supported via funding from Prince Sattam bin Abdulaziz University project number (PSAU/2023/R/1445).

Appendix A. Supplementary data

Supplementary data to this article can be found online at https://doi.org/10.1016/j.solidstatesciences.2023.107435.

References

[1] Y.M. Odeh, S.M. Azar, A.Y. Al-Reyahi, A.A. Mousa, E.K. Jaradat, N. Al Aqtash, Tuning the bandgap of cubic and orthorhombic BaZrS3 by substituting sulfur with selenium, AIP Adv. 13 (2023), https://doi.org/10.1063/5.0156875.
[2] L. Huang, W.R.L. Lambrecht, Electronic band structure, phonons, and exciton binding energies of halide perovskites CsSnCl3, CsSnBr3, and CsSnI3, Phys. Rev. B 88 (2013) 165203, https://doi.org/10.1103/PhysRevB.88.165203.
[3] D.B. Mitzi, Templating and structural engineering in organic–inorganic perovskites, J. Chem. Soc., Dalton Trans. (2001) 1–12, https://doi.org/10.1039/b007070j.
[4] S. Idrissi, H. Labrim, L. Bahmad, A. Benyoussef, Study of the solar perovskite CsMBr3 (M=Pb or Ge) photovoltaic materials: band-gap engineering, Solid State Sci. 118 (2021) 106679, https://doi.org/10.1016/j.solidstatesciences.2021.106679.
[5] D.R. Lawati, H.K. Neupane, D.K. Chaudhary, P. Shrestha, R.P. Adhikari, L.P. Joshi, R. Parajuli, Structural, mechanical, electronic and optical properties of MgZnO3 perovskite: first-principles study, J. Phys. Chem. Solid. 181 (2023) 111547, https://doi.org/10.1016/j.jpcs.2023.111547.
[6] G. Thiele, H.W. Rotter, K.D. Schmidt, Kristallstrukturen und Phasentransformationen von Caesiumtrihalogenogermanaten(II) CsGeX3 (X = Cl, Br, I), Z. Anorg. Allg. Chem. 545 (1987) 148–156, https://doi.org/10.1002/zaac.19875450217.
[7] S.S.I. Almishal, O. Rashwan, First-principles investigation of lead-free trigonal CsGeI3-xBrx mixed-halide perovskite system for optoelectronic applications: electronic and optical properties, Mater. Sci. Semicond. Process. 151 (2022) 107017, https://doi.org/10.1016/j.mssp.2022.107017.
[8] Y. Selmani, M. Mouatassime, F. Goumrhar, H. Labrim, L. Bahmad, A. Benyoussef, Structural, electronic and magnetic properties of the perovskite Ymno3, Solid State Commun. 328 (2021) 114254, https://doi.org/10.1016/j.ssc.2021.114254.
[9] H. Labrim, Y. Selmani, S. Ziti, S. Idrissi, R. El Bouayadi, D. Zejli, L. Bahmad, Study of the perovskites CaZrO3-xSx (x=0, 1, 2 and 3) for photovoltaic applications, Solid State Commun. 363 (2023) 115105, https://doi.org/10.1016/j.ssc.2023.115105.
[10] Y. Selmani, H. Labrim, S. Ziti, L. Bahmad, Electronic, optical and thermoelectric properties of the CsMF3 (M= Si or Ge) fluoro-perovskites, Comput. Condens. Matter. 32 (2022) e00699, https://doi.org/10.1016/j.cocom.2022.e00699.
[11] Y. Selmani, M. Mouatassime, F. Goumrhar, H. Labrim, L. Bahmad, A. Benyoussef, Structural, electronic and magnetic properties of the perovskite Ymno3, Solid State Commun. 328 (2021) 114254, https://doi.org/10.1016/j.ssc.2021.114254.
[12] Y. Selmani, H. Labrim, M. Mouatassime, L. Bahmad, Structural, optoelectronic and thermoelectric properties of Cs-based fluoroperovskites CsMF3 (M= Ge, Sn or Pb), Mater. Sci. Semicond. Process. 152 (2022) 107053, https://doi.org/10.1016/j.mssp.2022.107053.
[13] H.D. Megaw, Crystal structure of double oxides of the perovskite type, Proc. Phys. Soc. 58 (1946) 133–152, https://doi.org/10.1088/0959-5309/58/2/301.
[14] V. Bhooshan Kumar, L. Gouda, Z. Porat, A. Gedanken, Sonochemical synthesis of CH3NH3PbI3 perovskite ultrafine nanocrystal sensitizers for solar energy applications, Ultrason. Sonochem. 32 (2016) 54–59, https://doi.org/10.1016/j.ultsonch.2016.02.012.
[15] D.B. Mitzi, Templating and structural engineering in organic–inorganic perovskites, J. Chem. Soc., Dalton Trans. (2001) 1–12, https://doi.org/10.1039/b007070j.
[16] A.G. Chynoweth, Surface space-charge layers in barium titanate, Phys. Rev. 102 (1956) 705–714, https://doi.org/10.1103/PhysRev.102.705.
[17] S. Idrissi, L. Bahmad, A. Benyoussef, DFT and TDDFT studies of structural, electronic and optical properties of the inorganic solar perovskites XPbBr 3 (X = Li or Na), Phase Transitions 95 (2022) 501–514, https://doi.org/10.1080/01411594.2022.2080064.
[18] S. Idrissi, O. Mounkachi, L. Bahmad, A. Benyoussef, Study of the electronic and opto-electronic properties of the perovskite KPbBr3 by DFT and TDDFT methods, Comput. Condens. Matter. 33 (2022) e00617, https://doi.org/10.1016/j.cocom.2021.e00617.
[19] S. Yang, Q. Han, L. Wang, Y. Zhou, F. Yu, C. Li, X. Cai, L. Gao, C. Zhang, T. Ma, Over 23% power conversion efficiency of planar perovskite solar cells via bulk heterojunction design, Chem. Eng. J. 426 (2021) 131838, https://doi.org/10.1016/j.cej.2021.131838.
[20] Z. Zheng, S. Wang, Y. Hu, Y. Rong, A. Mei, H. Han, Development of formamidinium lead iodide-based perovskite solar cells: efficiency and stability, Chem. Sci. 13 (2022) 2167–2183, https://doi.org/10.1039/D1SC04769H.
[21] C. Lu, X. Li, X. Guo, S. Fu, W. Zhang, H. Yuan, J. Fang, Efficient inverted CsPbI3 perovskite solar cells fabricated in common air, Chem. Eng. J. 452 (2023) 139495, https://doi.org/10.1016/j.cej.2022.139495.
[22] J.A. Steele, T. Braeckevelt, V. Prakasam, G. Degutis, H. Yuan, H. Jin, E. Solano, P. Puech, S. Basak, M.I. Pintor-Monroy, H. Van Gorp, G. Fleury, R.X. Yang, Z. Lin, H. Huang, E. Debroye, D. Chernyshov, B. Chen, M. Wei, Y. Hou, R. Gehlhaar, J. Genoe, S. De Feyter, S.M.J. Rogge, A. Walsh, E.H. Sargent, P. Yang, J. Hofkens,

V. Van Speybroeck, M.B.J. Roeffaers, An embedded interfacial network stabilizes inorganic CsPbI3 perovskite thin films, Nat. Commun. 13 (2022) 7513, https://doi.org/10.1038/s41467-022-35255-9.
[23] X. Sun, Z. Shao, Z. Li, D. Liu, C. Gao, C. Chen, B. Zhang, L. Hao, Q. Zhao, Y. Li, X. Wang, Y. Lu, X. Wang, G. Cui, S. Pang, Highly efficient CsPbI3/Cs1-xDMAxPbI3 bulk heterojunction perovskite solar cell, Joule 6 (2022) 850–860, https://doi.org/10.1016/j.joule.2022.02.004.
[24] T.V. Vu, A.A. Lavrentyev, B.V. Gabrelian, K.D. Pham, O.V. Parasyuk, N. M. Denysyuk, O.Y. Khyzhun, Electronic structure and optical constants of CsPbCl3: the effect of approaches within ab initio calculations in relation to X-ray spectroscopy experiments, Mater. Chem. Phys. 261 (2021) 124216, https://doi.org/10.1016/j.matchemphys.2020.124216.
[25] L.C. Tang, J.Y. Huang, C.S. Chang, M.H. Lee, L.Q. Liu, New infrared nonlinear optical crystal CsGeBr 3 : synthesis, structure and powder second-harmonic generation properties, J. Phys. Condens. Matter 17 (2005) 7275–7286, https://doi.org/10.1088/0953-8984/17/46/011.
[26] Q. Mahmood, M. Yaseen, M. Hassan, M.S. Rashid, I. Tlili, A. Laref, The first-principle study of mechanical, optoelectronic and thermoelectric properties of CsGeBr 3 and CsSnBr 3 perovskites, Mater. Res. Express 6 (2019) 045901, https://doi.org/10.1088/2053-1591/aaf997.
[27] L.-C. Tang, C.-S. Chang, L.-C. Tang, J.Y. Huang, Electronic structure and optical properties of rhombohedral CsGeI 3 crystal, J. Phys. Condens. Matter 12 (2000) 9129–9143, https://doi.org/10.1088/0953-8984/12/43/303.
[28] P. Blaha, K. Schwarz, F. Tran, R. Laskowski, G.K.H. Madsen, L.D. Marks, WIEN2k: An APW+lo program for calculating the properties of solids, J. Chem. Phys. 152 (2020) 074101, https://doi.org/10.1063/1.5143061.
[29] K. Berarma, S.S. Essaoud, A.A. Mousa, S.M. Azar, A.Y. Al-Reyahi, Opto-electronic, thermodynamic and charge carriers transport properties of Ta $_2$ FeNiSn $_2$ and Nb $_2$ FeNiSn $_2$ double half-Heusler alloys, Semicond. Sci. Technol. 37 (2022) 055013, https://doi.org/10.1088/1361-6641/ac612b.
[30] A.Y. Al-Reyahi, S. Al Azar, A.A. Mousa, S.S. Essaoud, M. Maghrabi, K. Berarma, A. Aqili, A. Mufleh, H.I. Abu Radwan, Investigation of electronic, optical, and thermoelectric properties of half-metallic spinel X2NO4 (X=B, Al): first-principles calculations, Comput. Condens. Matter. 34 (2023) e00787, https://doi.org/10.1016/j.cocom.2023.e00787.
[31] S.S. Essaoud, S.M. Azar, A.A. Mousa, A.Y. Al-Reyahi, DFT-based investigation of electronic-structure, magnetic and thermoelectric properties of Dy $_2$ CoMnO $_6$ double perovskite, Phys. Scripta 98 (2023) 075930, https://doi.org/10.1088/1402-4896/acdd2c.
[32] N. Al Aqtash, A.Y. Al-Reyahi, S. Alnemrat, A.A. Twal, Stoichiometric and reduced ceria surfaces: atomic structure, energetics and electron localization, Comput. Theor. Chem. (2023) 114157, https://doi.org/10.1016/j.comptc.2023.114157.
[33] M. Maghrabi, A.Y. Al-Reyahi, N. Al Aqtash, S.M. Al Azar, A. Shaheen, A. Mufleh, B. Shaban, Investigating the physical properties of lead-free halide double perovskites Cs2AgXBr6 (X = P, As, Sb) for photovoltaic and thermoelectric devices using the density functional theory, Mater. Today Commun. 37 (2023) 107541, https://doi.org/10.1016/j.mtcomm.2023.107541.
[34] S. Saad Essaoud, S. Al Azar, A.A. Mousa, A.Y. Al-Reyahi, N. Al Aqtash, M.E. Ketfi, Insight into physical properties of lutetium-based double half-Heusler alloys LuXCo2Bi2 (X = V, Nb and Ta), J. Rare Earths (2023), https://doi.org/10.1016/j.jre.2023.11.011.
[35] M.E. Ketfi, S.S. Essaoud, S.M. Al Azar, A.Y. Al-Reyahi, A.A. Mousa, N. Al-Aqtash, Mechanical, magneto-electronic and thermoelectric properties of Ba 2 MgReO 6 and Ba 2 YMoO 6 based cubic double perovskites: an ab initio study, Phys. Scripta 99 (2023) 015908, https://doi.org/10.1088/1402-4896/ad1021.
[36] D. Koller, P. Blaha, F. Tran, Hybrid functionals for solids with an optimized Hartree–Fock mixing parameter, J. Phys. Condens. Matter 25 (2013) 435503, https://doi.org/10.1088/0953-8984/25/43/435503.
[37] K. Radja, B.L. Farah, A. Ibrahim, D. Lamia, I. Fatima, B. Nabil, A. Mohamed, Y. Al-Douri, A.F.A. El-Rehim, Investigation of structural, magneto-electronic, elastic, mechanical and thermoelectric properties of novel lead-free halide double perovskite Cs2AgFeCl6: first-principles calculations, J. Phys. Chem. Solid. 167 (2022) 110795, https://doi.org/10.1016/j.jpcs.2022.110795.
[38] F. Tran, P. Blaha, Implementation of screened hybrid functionals based on the Yukawa potential within the LAPW basis set, Phys. Rev. B 83 (2011) 235118, https://doi.org/10.1103/PhysRevB.83.235118.
[39] F. Tran, P. Blaha, M. Betzinger, S. Blügel, Comparison between exact and semilocal exchange potentials: an all-electron study for solids, Phys. Rev. B Condens. Matter 91 (2015), https://doi.org/10.1103/PhysRevB.91.165121.
[40] F. Birch, Finite strain isotherm and velocities for single-crystal and polycrystalline NaCl at high pressures and 300°K, J. Geophys. Res. 83 (1978) 1257, https://doi.org/10.1029/JB083iB03p01257.
[41] M.E. Ketfi, S.S. Essaoud, S. Al Azar, A.Y. Al-Reyahi, A.A. Mousa, A. Mufleh, Insight into the spin-polarized structural, optoelectronic, magnetic, thermodynamic, and thermoelectric properties of PdBO2 (B = Al, Cr, and Rh) Delafossite semiconductor, Opt. Quant. Electron. 55 (2023) 1013, https://doi.org/10.1007/s11082-023-05259-w.
[42] S.S. Essaoud, S.M. Azar, A.A. Mousa, A.Y. Al-Reyahi, DFT-based investigation of electronic-structure, magnetic and thermoelectric properties of Dy 2 CoMnO 6 double perovskite, Phys. Scripta 98 (2023) 075930, https://doi.org/10.1088/1402-4896/acdd2c.
[43] A. Najim, B. Hartiti, H. Absike, H.J. Tchognia Nkuissi, H. Labrim, S. Fadili, P. Thevenin, M. Ertugrul, Theoretical investigation of structural, electronic, and optical properties of halide cubic perovskite CsPbBr3-xIx, Mater. Sci. Semicond. Process. 141 (2022) 106442, https://doi.org/10.1016/j.mssp.2021.106442.
[44] A. Togo, I. Tanaka, First principles phonon calculations in materials science, Scripta Mater. 108 (2015) 1–5, https://doi.org/10.1016/j.scriptamat.2015.07.021.
[45] Y.-Y. Yang, P. Gong, W.-D. Ma, R. Hao, X.-Y. Fang, Effects of substitution of group-V atoms for carbon or silicon atoms on optical properties of silicon carbide nanotubes, Chin. Phys. B 30 (2021) 067803, https://doi.org/10.1088/1674-1056/abdb1e.
[46] A.M. Mebed, M. Mushtaq, I. Muhammad, I.U.N. Lone, S. Al-Qaisi, N. Algethami, E. F. El-Shamy, A. Laref, N.M. Al-Hosiny, Structure, half-metallic and magnetic properties of bulk and (001) surface of Rb 2 XMoO 6 (X = Cr, Sc) double perovskites: a DFT + U study, Phys. Scripta 98 (2023) 015807, https://doi.org/10.1088/1402-4896/aca56b.
[47] L. Huang, W.R.L. Lambrecht, Electronic band structure trends of perovskite halides: beyond Pb and Sn to Ge and Si, Phys. Rev. B 93 (2016) 195211, https://doi.org/10.1103/PhysRevB.93.195211.
[48] T.V. Vu, A.A. Lavrentyev, B.V. Gabrelian, V.A. Ocheretova, O.V. Parasyuk, O. Y. Khyzhun, Particular features of the electronic structure and optical properties of Ag2PbGeS4 as evidenced from first-principles DFT calculations and XPS studies, Mater. Chem. Phys. 208 (2018) 268–280, https://doi.org/10.1016/j.matchemphys.2018.01.042.
[49] A.A. Lavrentyev, B.V. Gabrelian, V.T. Vu, P.N. Shkumat, G.L. Myronchuk, M. Khvyshchun, A.O. Fedorchuk, O.V. Parasyuk, O.Y. Khyzhun, Electronic structure and optical properties of Cs2HgI4: experimental study and band-structure DFT calculations, Opt. Mater. 42 (2015) 351–360, https://doi.org/10.1016/j.optmat.2015.01.026.
[50] L.-C. Tang, Y.-C. Chang, J.-Y. Huang, M.-H. Lee, C.-S. Chang, First principles calculations of linear and second-order optical responses in rhombohedrally distorted perovskite ternary halides, CsGeX 3 (X = Cl, Br, and I), Jpn. J. Appl. Phys. 48 (2009) 112402, https://doi.org/10.1143/JJAP.48.112402.
[51] D. Shanthi, P. Selvarajan, S. Perumal, Growth, linear optical constants and photoluminescence characteristics of beta-alaninium picrate (BAP) crystals, Optik 127 (2016) 3192–3199, https://doi.org/10.1016/j.ijleo.2015.11.189.
[52] B. Meyer, D. Vanderbilt, Ab initio study of BaTiO 3 and PbTiO 3 surfaces in external electric fields, Phys. Rev. B 63 (2001) 205426, https://doi.org/10.1103/PhysRevB.63.205426.
[53] D.R. Penn, Electron mean-free-path calculations using a model dielectric function, Phys. Rev. B 35 (1987) 482–486, https://doi.org/10.1103/PhysRevB.35.482.
[54] N. Al Aqtash, S.M. Al Azar, A.Y. Al-Reyahi, A. Mufleh, M. Maghrabi, S.S. Essaoud, K. Berarma, A.A. Mousa, First-principles calculations to investigate structural, mechanical, electronic, optical, and thermoelectric properties of novel cubic double Perovskites X2AgBiBr6 (X=Li, Na, K, Rb, Cs) for optoelectronic devices, Mol. Simulat. (2023) 1–12, https://doi.org/10.1080/08927022.2023.2251604.
[55] A.I. Arbab, On the optical conductivity, Optik 194 (2019) 163067, https://doi.org/10.1016/j.ijleo.2019.163067.
[56] N. Smith, Classical generalization of the Drude formula for the optical conductivity, Phys. Rev. B 64 (2001) 155106, https://doi.org/10.1103/PhysRevB.64.155106.
[57] M. Sohail, M. Husain, N. Rahman, K. Althubeiti, M. Algethami, A.A. Khan, A. Iqbal, A. Ullah, A. Khan, R. Khan, First-principal investigations of electronic, structural, elastic and optical properties of the fluoroperovskite TlLF 3 (L = Ca, Cd) compounds for optoelectronic applications, RSC Adv. 12 (2022) 7002–7008, https://doi.org/10.1039/D2RA00464J.
[58] J. Sun, X.F. Zhou, Y.X. Fan, J. Chen, H.T. Wang, X. Guo, J. He, Y. Tian, First-principles study of electronic structure and optical properties of heterodiamond BC2 N, Phys. Rev. B Condens. Matter 73 (2006), https://doi.org/10.1103/PhysRevB.73.045108.
[59] M.I. Khan, B. Mehmood, M.A. Naeem, M. Younis, K.H. Mahmoud, Z.M. El-Bahy, W. S. Subhani, S. Hussain, N. Alwadai, H. Albalawi, M. Iqbal, Investigations the structural, optical and photovoltaic properties of La doped TiO2 photoanode based dye sensitized solar cells, Opt. Mater. 122 (2021) 111610, https://doi.org/10.1016/j.optmat.2021.111610.
[60] H. Chen, H. Huang, X. Huang, J.N. Clifford, A. Forneli, E. Palomares, X. Zheng, L. Zheng, X. Wang, P. Shen, B. Zhao, S. Tan, High molar extinction coefficient branchlike organic dyes containing di(p -tolyl)phenylamine donor for dye-sensitized solar cells applications, J. Phys. Chem. C 114 (2010) 3280–3286, https://doi.org/10.1021/jp911139x.
[61] M. Aslam, A. Khan, M.A. Hashmi, M. Sajjad, E. Algrafy, G.M. Mustafa, A. Mahmood, S.M. Ramay, Physical characteristics of CdZrO3 perovskite at different pressure for optoelectronic application, J. Mater. Res. Technol. 9 (2020) 9965–9971, https://doi.org/10.1016/j.jmrt.2020.06.086.
[62] R.Kr Giri, S.H. Chaki, M.S. Dave, S.R. Bharucha, A.J. Khimani, R.M. Kannaujiya, M. P. Deshpande, M.B. Solanki, First principle insights and experimental investigations of the electronic and optical properties of CuInS 2 single crystals, Mater. Adv. 4 (2023) 3246–3256, https://doi.org/10.1039/D3MA00166K.
[63] B. Yang, C. Li, Z. Wang, Q. Dai, Thermoplasmonics in solar energy conversion: materials, nanostructured designs, and applications, Adv. Mater. 34 (2022), https://doi.org/10.1002/adma.202107351.